Transactions of JASCOME, Journal of Boundary Element Methods, Vol. 21 (Dec. 2004), No. 08-040927 JASCOME

FAST HYBRID BNM ANALYSIS OF HEAT CONDUCTION PROPERTIES OF CNT-BASED COMPOSITES

Masataka TANAKA [1], Jianming ZHANG [2], Morinobu ENDO [3]

1) Faculty of Engineering, Shinshu University, (Nagano 380-8553, e-mail: dtanaka@gipwc.shinshu-u.ac.jp)

2) Faculty of Engineering, Shinshu University, (Nagano 380-8553, e-mail: zhangjm@homer.shinshu-u.ac.jp)

3) Faculty of Engineering, Shinshu University, (Nagano 380-8553, e-mail: endo@endomoribu.shinshu-u.ac.jp)

The equivalent heat conductivity of the carbon nanotube (CNT) composites is usually evaluated using a representative volume element (RVE) with one or several CNTs embedded. For realistic modeling a large number of CNTs included in the RVE are necessary. However, analysis of such an RVE using mesh-based methods may face severe difficulties in discretization of the geometry. In this paper, the numerical method of choice is the hybrid boundary node method (Hybrid BNM), due to its boundary-only and meshless nature. To deal with the extremely large computational scale, the Hybrid BNM can be accelerated by fast multipole method (FMM) based on a simplified mathematical model which has been proposed especially for thermal analysis of CNT-based composites. A computer code written in C++ is developed and then employed for computing RVEs containing a number of CNTs with different alignments. It is concluded that some specific alignments may significantly increase the equivalent heat conductivity

Keywords: hybrid boundary node method; CNT-based composites; fast multipole method; heat conduction

1. Introduction

Carbon nanotubes (CNT) possess exceptional physical properties such as superior thermal and electrical conductivities, as well as high stiffness and strength [1]. These remarkable physical properties make CNTs promising in engineering applications, such as development of fundamentally new composite materials, and heat transport management in miniature device components. CNT-based composites offer significant improvements to performance over their base polymers. This study aims at gaining insight into the thermal properties of CNT-based composites through numerical simulation. The equivalent heat conductivity of carbon nanotube-based composites is evaluated using a representative volume element (RVE) based on 3-D potential theory.

For the analysis of an RVE in which not only single but many CNTs are randomly distributed, the implementation of standard numerical solution techniques like FEM or BEM may face severe difficulties in discretization of the domain geometry in question. This is valid especially for FEM models where meshing of the solid geometries within CNT-reinforced polymers may be tedious and extremely difficult. To alleviate this difficulty the hybrid boundary node method (Hybrid BNM) can be used [2]. By combining a modified functional with the moving least squares (MLS) approximation, the Hybrid BNM is a truly meshless, boundary-only method. We have combined the Hybrid BNM with a multi-domain solver and applied the combined approach to perform some preliminary computations and investigate the influences of the CNT length, curvature and dispersion on the equivalent thermal properties of the composites [3, 4].

However, these computations are limited to relatively small scales, as usually only single or several but shorter CNTs were considered. Due to the very thin and slender structure of the CNTs, a large number of nodes are required to discretize them in order to capture the steep gradients. Moreover, in a multi-domain solver, at each node on the interface of a CNT with the host polymer, both temperature and normal flux are unknown. This situation considerably increases the total degrees of freedom in the overall system of equations.

The preliminary studies have also shown that temperatures within the entire CNT are almost uniform due to the huge difference of heat conductivity between the CNT and the host polymer. Based on this observation, we have proposed a simplified mathematical model, where the CNTs are considered as heat superconductors and uniform temperature distributions within the entire body of each CNT assumed [5]. As a result, the total number of degrees of freedom is reduced by half, and thus increases the number of CNTs contained in an RVE that can be analyzed within available computer resources. The simplified model has been rigorously tested and validated using benchmark examples.

Nevertheless, even with the simplified model, both the memory requirements and the computational scale are still of $O(N^2)$, (when an iterative solver applied, if a direct solver, the Gauss elimination for example, is used, the computational scale is even higher up to $O(N^3)$), where N stands for the total number of degrees of freedom. To perform analysis of a real-world RVE model, an efficient technique further reducing computational requirements is necessary. The method of choice is FMM.

The FMM was introduced by Rokhlin [6], and developed by Greengard [7] as an algorithm for the rapid evaluation of Coulombic interactions in a large scale ensemble of particles. In their method, multipole moments are used to represent distant particle groups, a local expansion to evaluate the contribution from distant particles in the form of a series, and a hierarchical decomposition of the domain to carry out efficient and systematic grouping of the particles. The FMM reduces both memory size and computational scale from $O(N^2)$ to $O(N)$, thus enabling scientific and engineering computations that were previously impossible.

The FMM has been applied to a variety of computation methods. Applying FMM to accelerate BEM computation has been investigated by many researchers [8]. In this paper, the FMM techniques are implemented into the Hybrid BNM based on the simplified model for simulation of thermal behavior of CNT-based composites. RVEs containing a number of CNTs with different lengths, shapes and alignments, have been studied. It is realized that some specific alignments may significantly increase the equivalent heat conductivity of the composites.

2. Hybrid BNM formulation for the simplified model

As mentioned in the introduction, the unusually high heat conductivity of the CNTs in comparison with the polymer makes the temperature distribution within an individual CNT almost uniform. This feature allows us to simplify the modeling of the CNT-based composites. In this section the formulations for the simplified mathematical model are developed, where only single domain, namely the polymer matrix is modeled. Each CNT is treated as a heat superconductor with one constant temperature constrained at its surface. A similar assumption can be found in a rigid-line inclusion model [9].

Suppose that n CNTs are distributed in a polymer matrix which makes an RVE. It is assumed that the matrix is continua of linear, isotropic and homogenous materials with given heat conductivities. A steady state heat conduction problem governed by Laplace's equation with proper boundary conditions is considered.

The Hybrid BNM is based on a modified variational principle, in which there are three independent variables, namely:

- temperature within the domain, ϕ;
- boundary temperature, $\tilde{\phi}$;
- boundary normal heat flux, $\tilde{q}$.

Suppose further that N nodes are randomly distributed on the surfaces (including the interfaces with CNTs) of the polymer domain. The temperature within the domain is approximated using fundamental solutions as follows:

$$\phi = \sum_{J=1}^{N} \phi_J^s x_J \tag{1}$$

and hence the normal heat flux is given by:

$$q = -\kappa \sum_{J=1}^{N} \frac{\partial \phi_J^s}{\partial n} x_J \tag{2}$$

where ϕ_J^s is the fundamental solution with the source at a node $\mathbf{s}_J$, κ is the heat conductivity and x_J are unknown parameters. For 3-D steady state heat conduction problems, the fundamental solution can be written as

$$\phi_J^s = \frac{1}{\kappa} \frac{1}{4\pi r(Q, \mathbf{s}_J)} \tag{3}$$

where Q is a field point; $r(Q, \mathbf{s}_J)$ is the distance between Q and $\mathbf{s}_J$.

The boundary temperature and normal heat flux are approximated by moving least square (MLS) approximation:

$$\tilde{\phi}(\mathbf{s}) = \sum_{J=1}^{N} \Phi_J(\mathbf{s}) \hat{\phi}_J \tag{4}$$

and

$$\tilde{q}(\mathbf{s}) = \sum_{J=1}^{N} \Phi_J(\mathbf{s}) \hat{q}_J \tag{5}$$

In the foregoing equations, $\Phi_J(\mathbf{s})$ is the shape function of MLS approximation; $\hat{\phi}_J$ and $\hat{q}_J$ are nodal values of temperature and normal flux, respectively.

For the polymer domain, the following set of Hybrid BNM equations can be written:

$$\begin{bmatrix} U_{00} & U_{01} & \cdots & U_{0n} \\ U_{10} & U_{11} & \cdots & U_{1n} \\ \vdots & \vdots & \ddots & \vdots \\ U_{n0} & U_{n1} & \cdots & U_{nn} \end{bmatrix} \begin{Bmatrix} x_0 \\ x_1 \\ \vdots \\ x_n \end{Bmatrix} = \begin{Bmatrix} H_0 \hat{\phi}_0 \\ H_1 \hat{\phi}_1 \\ \vdots \\ H_n \hat{\phi}_n \end{Bmatrix} \tag{6}$$

$$\begin{bmatrix} V_{00} & V_{01} & \cdots & V_{0n} \\ V_{10} & V_{11} & \cdots & V_{1n} \\ \vdots & \vdots & \ddots & \vdots \\ V_{n0} & V_{n1} & \cdots & V_{nn} \end{bmatrix} \begin{Bmatrix} x_0 \\ x_1 \\ \vdots \\ x_n \end{Bmatrix} = \begin{Bmatrix} H_0 \hat{q}_0 \\ H_1 \hat{q}_1 \\ \vdots \\ H_n \hat{q}_n \end{Bmatrix} \tag{7}$$

where subscripts 0 and $k\,(=1,\cdots,n)$, stand for quantities exclusively associated with the polymer domain, and quantities associated with its interface with the k-th nanotube, respectively. The sub-matrices $[U]$, $[V]$ and $[H]$ are given as:

$$U_{IJ} = \int_{\Gamma_I} \phi_J^s v_I(Q) d\Gamma \tag{8}$$

$$V_{IJ} = -\kappa \int_{\Gamma_I} \frac{\partial \phi_J^s}{\partial n} v_I(Q) d\Gamma \tag{9}$$

$$H_{IJ} = \int_{\Gamma_I} \Phi_J(\mathbf{s}) v_I(Q) d\Gamma \tag{10}$$

where Γ_I is a regularly shaped local region around a collocation node $\mathbf{s}_I$, v_I is a weight function and $\mathbf{s}$ is a field point on the boundary. For full details of Hybrid BNM refer to [2].

By combining Eqs. (6) and (7), we have the following equation:

$$\begin{bmatrix} A_{00} & A_{01} & \cdots & A_{0n} \\ U_{10} & U_{11} & \cdots & U_{1n} \\ \vdots & \vdots & \ddots & \vdots \\ U_{n0} & U_{n1} & \cdots & U_{nn} \end{bmatrix} \begin{Bmatrix} x_0 \\ x_1 \\ \vdots \\ x_n \end{Bmatrix} = \begin{Bmatrix} H_0 d_0 \\ H_1 \hat{\phi}_1 \\ \vdots \\ H_n \hat{\phi}_n \end{Bmatrix} \tag{11}$$

where, each row of sub-matrices $[A_{0k}], k = 0,1,\cdots,n$, is supplied identically from that in $[U_{0k}]$ or $[V_{0k}]$ according to the boundary condition at the corresponding node, and the corresponding term of $\{d_0\}$ comes from $\{\hat{\phi}_0\}$ or $\{\hat{q}_0\}$.

Further suppose that m_k nodes are located at the interface of k-th nanotube with the polymer, and a constant temperature ϕ_c^k is prescribed, namely

$$\left\{\hat{\phi}_k\right\} = \{\mathbf{1}\}_k \phi_c^k \tag{12}$$

where $\left\{\hat{\phi}_k\right\}$ is the nodal values of temperature at the interface; $\{\mathbf{1}\}_k$ is a column vector of m_k dimensions with all the elements equal 1. Inserting Eq. (12) into Eq. (11) for all interfaces, the following equation is obtained,

$$\begin{bmatrix} A_{00} & A_{01} & \cdots & A_{0n} & \mathbf{0} & \cdots & \mathbf{0} \\ U_{10} & U_{11} & \cdots & U_{1n} & -H_1\{\mathbf{1}\}_1 & \cdots & \mathbf{0} \\ \vdots & \vdots & \ddots & \vdots & \vdots & \ddots & \vdots \\ U_{n0} & U_{n1} & \cdots & U_{nn} & \mathbf{0} & \cdots & -H_n\{\mathbf{1}\}_n \end{bmatrix} \begin{Bmatrix} x_0 \\ x_1 \\ \vdots \\ x_n \\ \phi_c^1 \\ \vdots \\ \phi_c^n \end{Bmatrix} = \begin{Bmatrix} H_0 d_0 \\ \mathbf{0} \\ \vdots \\ \mathbf{0} \end{Bmatrix} \tag{13}$$

In the above set of equations, there are n (the number of CNTs) more unknowns than the number of equations, because we have introduced one additional unknown, i.e. the constant temperature, for each CNT. In order to solve Eq. (13), we have to add n extra equations. These equations can be obtained from energy conservation law. Actually, in steady state heat conduction, the rate of thermal energy flowing into a CNT must equal that flowing out. Therefore, the following relationship exists at the surface of the k-th CNT,

$$\int_{C_k} q d\Gamma = 0 \tag{14}$$

where C_k represents the outer surface of the k-th CNT. Substituting Eq. (2) into (14) and omitting the common factor κ, we have

$$\sum_{J=1}^{N} \int_{C_k} \frac{\partial \phi_J^s}{\partial n} d\Gamma \, x_J = 0 \tag{15}$$

In Eq. (15), C_k is a closed surface. The following integral identity [10] holds,

$$\int_{C_k} \frac{\partial \phi_J^s}{\partial n} d\Gamma = \begin{cases} 1, & \forall \mathbf{s}_J \in C_k \\ 0, & \forall \mathbf{s}_J \notin C_k \end{cases} \tag{21}$$

Therefore, the coefficients in Eq. (15) are either 1 or 0. For nodes located on the surface of the k-th CNT, they are 1, otherwise they are 0. Appending Eq. (15) to Eq. (13) for all CNTs, we obtain the final set of algebraic equations system which can uniquely determine the unknown parameter $\boldsymbol{x}$.

$$\begin{bmatrix} A_{00} & A_{01} & \cdots & A_{0n} & \mathbf{0} & \cdots & \mathbf{0} \\ U_{10} & U_{11} & \cdots & U_{1n} & -H_1\{\mathbf{1}\}_1 & \cdots & \mathbf{0} \\ \mathbf{0} & \{\mathbf{1}\}_1^{\mathrm{T}} & \cdots & \mathbf{0} & 0 & \cdots & 0 \\ \vdots & \vdots & \ddots & \vdots & \vdots & \ddots & \vdots \\ U_{n0} & U_{n1} & \cdots & U_{nn} & \mathbf{0} & \cdots & -H_n\{\mathbf{1}\}_n \\ \mathbf{0} & \mathbf{0} & \cdots & \{\mathbf{1}\}_n^{\mathrm{T}} & 0 & \cdots & 0 \end{bmatrix} \begin{Bmatrix} x_0 \\ x_1 \\ \vdots \\ x_n \\ \phi_c^1 \\ \vdots \\ \phi_c^n \end{Bmatrix} = \begin{Bmatrix} H_0 d_0 \\ \mathbf{0} \\ 0 \\ \vdots \\ \mathbf{0} \\ 0 \end{Bmatrix} \tag{17}$$

The total number of degrees of freedom in Eq. (17) is relatively very small when compared with that of a full model (multi-domain solver, see [5]). For each CNT, only one algebraic equation is added. Moreover, as the coefficients of these algebraic equations are either 1 or 0, calculations of them are avoided. Therefore, both the CPU time and memory usage can be saved significantly.

The set of Eq. (17) is solved for the unknown parameters $\boldsymbol{x}$, and then, by back-substitution into Eqs. (6) and (7), the boundary unknowns are obtained either on the interfaces or the external boundary surfaces. As demonstrated, the Hybrid BNM is a boundary-only meshless approach. No boundary elements are used for either interpolation or integration purposes. Therefore, it may alleviate the discretization task to a large extent for complicated geometries.

3. Accelerating equation solution by FMM

The size of the coefficient matrix in Eq. (17) is dominated by sub-matrices $\left[A_{0k}\right]$ and $\left[U_{ki}\right]$, $k = 1, \cdots, n$, $i = 0, 1, \cdots, n$. Since these sub-matrices are unsymmetrical and fully populated, solving Eq. (17) by an iterative solver requires $O(N^2)$ operations. In this paper, we use the restarted preconditioned GMRES to solve Eq. (17). The most time-consuming aspect of an iterative method when employed for solving a system of linear equations is the matrix-vector product in each iteration step. Taking an iteration vector $\mathbf{x}'$ into account, the product of a row of the coefficient matrix in Eq. (17) and the guess vector $\mathbf{x}'$ can be expressed as one of the following four sums:

$$\sum_{J=1}^{N} \int_{\Gamma_J} \phi_J^s v_I(Q) x_J' d\Gamma \tag{18}$$

$$\sum_{J=1}^{N} \int_{\Gamma_J} -\kappa \frac{\partial \phi_J^s}{\partial n} v_I(Q) x_J' d\Gamma \tag{19}$$

$$\sum_{J=1}^{N} \int_{\Gamma_J} \phi_J^s v_I(Q) x_J' d\Gamma + \phi_c^k \sum_{J}^{m_k} H_{IJ} \tag{20}$$

$$\sum_{J}^{m_k} x_J^k \tag{21}$$

Sums (18) and (19) are related to a node located on the external boundary and prescribed with temperature and normal flux, respectively. Sum (20) is related to a node located at the interface of the k-th CNT with the polymer domain, and Expression (21) to the k-th uniform temperature constraint.

The computational costs for the second term in sum (20) and sum (21) are trivial, and can be ignored. This section will mainly focus on how to accelerate summations (18) and (19) by means of FMM. For this purpose, we first construct a hierarchy of boxes which refine the computational domain into smaller and smaller regions. At refinement level 0, we have the entire computational domain. Refinement level l+1 is obtained recursively from level l by subdivision of each into eight equal parts. This yields a natural tree structure, where the eight boxes at level l+1 obtained by subdivision of a box at level l are considered its children. We stop the box subdivision if the number of nodes included in the box is smaller than a given value. If a child box contains no node, we delete it. A childless box is called a leaf. We call two boxes *neighbors* if they are at the same level and share at least a vertex, or *well separated* when they are at the same level but not neighbors. With each box b we associate an *interaction list*, consisting of the children of the neighbors of b's parent which are well separated from box b.

For simplicity only, we will ignore for a moment the summation (19). Suppose the boundary node $\mathbf{s}_J$ belongs to a

leaf of the hierarchical tree of boxes. We divide sum (18) into two parts: the sum of the contributions of the nodes contained in the neighbors of the leaf (these nodes are called near nodes), and that of the nodes that are outside all the neighbors (these nodes are called far nodes). Eq. (18) can then be rewritten as [7]

$$\sum_{J=1}^{N} \int_{\Gamma_J} \phi_j^s v_l(Q) x_j' d\Gamma = \sum_{j}^{N_{near}} \int_{\Gamma_J} \phi_j^s v_l(Q) x_j' d\Gamma + \sum_{j}^{N_{far}} \int_{\Gamma_J} \phi_j^s v_l(Q) x_j' d\Gamma \quad (22)$$

where N_{near} and N_{far} are the numbers of the near nodes and far nodes, respectively.

We will compute the sum for the near nodes directly, while use multipole expansions to speed up the summation for the far nodes. Consider two leafs B_{far} and B_{local} which are well separated. B_{local} contains node $\mathbf{s}_l$ and B_{far} contains N_b nodes. The fundamental solution is first expanded into a spherical harmonic series as

$$\phi_j^s = \frac{1}{4\pi} \frac{1}{r(Q,\mathbf{s}_j)} = \frac{1}{4\pi} \sum_{n=0}^{\infty} \sum_{m=-n}^{n} \rho^n Y_n^{-m}(\alpha,\beta) \frac{Y_n^m(\theta,\phi)}{r^{n+1}} \quad (23)$$

where (r,θ,ϕ) and (ρ,α,β) are the spherical coordinates of Q and $\mathbf{s}_j$, respectively, with the origin of the coordinate system located at the center of B_{far}. Obviously, $r > \rho$. The function $Y_n^m(x,y)$ is defined by

$$Y_n^m(x,y) = \sqrt{\frac{(n-|m|)!}{(n+|m|)!}} P_n^{|m|}(\cos x) e^{imy}$$

with P_n^m defined by Rodrigues' formula (see [7]).

Then, the far field sum in (22) for the nodes inside B_{far} can be obtained by

$$\sum_{j}^{N_b} \int_{\Gamma_l} \phi_j^s v_l(Q) x_j' d\Gamma = \frac{1}{4\pi} \sum_{n=0}^{\infty} \sum_{m=-n}^{n} M_n^m \int_{\Gamma_l} \frac{Y_n^m(\theta,\phi)}{r^{n+1}} v_l(Q) d\Gamma \quad (24)$$

where M_n^m is called multipole moments and given by

$$M_n^m = \sum_{j}^{N_b} \rho_j^n Y_n^{-m}(\alpha_j,\beta_j) x_j' \quad (25)$$

Now we move the origin of the spherical coordinate system to the center of B_{local}, and suppose that the coordinates of B_{far}'s center and the node $\mathbf{s}_l$ are (r',θ',ϕ') and (ρ',α',β'), respectively, $Y_n^m(\theta,\phi)/r^{n+1}$ can be further expanded in terms of spherical harmonics as [7]

$$\frac{Y_n^m(\theta,\phi)}{r^{n+1}} = \sum_{j=0}^{\infty} \sum_{k=-j}^{j} \frac{i^{|k-m|-|k|-|m|} A_n^m A_j^k Y_{n+j}^{m-k}(\alpha',\beta')}{(-1)^n A_{n+j}^{m-k} \rho'^{j+n+1}} Y_j^k(\theta',\phi') r'^j$$

with A_n^m defined by

$$A_n^m = \frac{(-1)^n}{\sqrt{(n-m)!(n+m)!}}$$

Eq. (24) becomes

$$\sum_{j}^{N_b} \int_{\Gamma_l} \phi_j^s v_l(Q) x_j' d\Gamma = \sum_{j=0}^{\infty} \sum_{k=-j}^{j} L_j^k S_j^k \quad (26)$$

where L_j^k is given by

$$L_j^k = \sum_{n=0}^{\infty} \sum_{m=-n}^{n} M_n^m \frac{i^{|k-m|-|k|-|m|} A_n^m A_j^k Y_{n+j}^{m-k}(\alpha',\beta')}{(-1)^n A_{n+j}^{m-k} \rho'^{j+n+1}} \quad (27)$$

and

$$S_j^k = \frac{1}{4\pi} \int_{\Gamma_l} Y_j^k(\theta',\phi') r'^j v_l(Q)_j d\Gamma \quad (28)$$

As B_{far} and B_{local} are well separated, $\rho' > 2r'$ is guaranteed. Eq.(27) is usually called *far to near* translation. If B_{far} belongs to the interaction list of B_{local}, we compute the sum (26) using Eq. (26) directly. Else if B_{far}'s father belongs to the interaction list of B_{local}'s father, we first translate M_n^m into $M_j'^k$ which is about the center of B_{far}'s father, by [7]

$$M_j'^k = \sum_{n=0}^{j} \sum_{m=-n}^{n} M_{j-n}^{k-m} \frac{i^{|k|-|m|-|k-m|} A_n^m A_{j-n}^{k-m} \rho^n Y_n^{-m}(\alpha,\beta)}{A_j^k} \quad (29)$$

where (ρ,α,β) are coordinates of B_{far}'s center with the origin located at the center of B_{far}'s father.

We then translate $M_j'^k$ into L'^m_n by Eq. (27), finally translate L'^m_n into L_j^k from father to child using the following equation [7]:

$$L_j^k = \sum_{n=j}^{\infty} \sum_{m=-n}^{n} L'^m_n \frac{i^{|m|-|m-k|-|k|} A_{n-j}^{m-k} A_j^k Y_{n-j}^{m-k}(\alpha,\beta) \rho^{n-j}}{(-1)^{n+j} A_n^m} \quad (30)$$

where (ρ,α,β) are coordinates of B_{local}'s center with the origin located at the center of B_{local}'s father.

Eqs. (29) and (30) are called *far to far* and *near to near* translation, respectively.

If a box of B_{far}'s ancestor at level l belongs to the interaction list of B_{local}'s ancestor, the above process is recursively repeated until level l. This scheme guarantees that all the far to near conversions are performed between a box and its interaction list, and hence the condition $\rho' > 2r'$ required by Eq. (27) is ensured.

The computing process for the far field sum (19) is the same as sum (18), except that Eq. (26) is replaced by

$$\sum_{J}^{N_b} \int_{\Gamma_l} \frac{\partial \phi_j^s}{\partial n} v_l(Q) x_j' d\Gamma = \sum_{j=0}^{\infty} \sum_{k=-j}^{j} L_j^k \frac{\partial S_j^k}{\partial n} \quad (31)$$

where $\frac{\partial S_j^k}{\partial n}$ is given by

$$\frac{\partial S_j^k}{\partial n} = \frac{1}{4\pi} \int_{\Gamma_l} \frac{\partial Y_j^k(\theta',\phi') r'^j}{\partial n} v_l(Q) d\Gamma \quad (32)$$

So far we have described the process of summations (18) and (19) for a cluster of nodes contained in a leaf B_{far}, with respect to a node $\mathbf{s}_l$ included in another leaf B_{local} which is well separated from B_{far}. In actual computations, the summations are not performed separately for each pair of well separated boxes. Systematically, the fast multipole algorithm begins with the finest level, from where the multipole moments are shifted to the centers of the cubes and combined, so that a single expansion represents all of the nodes in the cube. During an *upward pass* through the tree to the root, each child cube's multipole expansions is shifted to its parent's center, to generate a single expansion which represents all of the nodes in the parent cube. In an *interaction phase*, at each level a local expansion is created for each cube by accumulating multipole expansions representing distant cubes at that level. In a *downward pass*, the local expansions in the parent cubes are shifted to the centers of their children. Finally, in an *evaluation phase*, the local expansions and direct contributions from nearby nodes are evaluated at the collocation points.

4. Study on thermal behavior of CNT-based composites

In this section, we use an RVE to study the CNT-based composites for their thermal properties. The RVE are modeled with straight or curved CNTs embedded, and with properly applied boundary conditions. A rectangular RVE is employed with the dimensions shown in Fig. 1. Based on the simplified mathematical model, the CNTs are treated as cavities which are identical to the outer surfaces of the CNTs. A constant temperature is constrained at a cavity surface. The radii of CNTs (R=5 nm) are kept constant in all the following examples, while their length and shapes, together with the number of CNTs and their alignments, varies for different examples. The heat conductivity, κ^p, used for the polymer (polycarbonate) is 0.37 W/m·K.

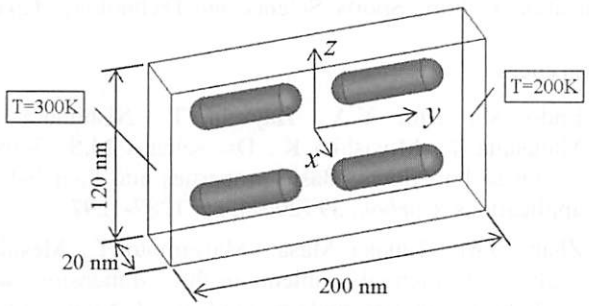

Figure 1: A Nanoscale RVE.

Computations are performed on a desktop computer with an Intel(R) Pentium(R) 4 CPU (1.99GHz). Following Reference [8], we truncate all the infinite expansions after p=10, set the maximum number of boundary nodes in a leaf box to be 60, and terminate the iteration when the relative error is less than 10^{-6}.

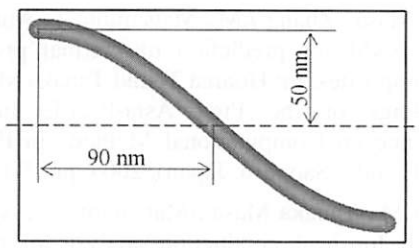

Figure 2: An RVE including a sinusoidal CNT.

4.1 Accuracy of the FMM

First, we will examine the accuracy of the proposed method. An RVE with a sinusoidal CNT embedded is used in this study. Fig. 2 shows the geometry. As there is no analytical solution existing for the simplified model, we impose Dirichlet boundary condition on all the surfaces, including cavity, according to the following exact solution:

$$u = x^3 + y^3 + z^3 - 3yx^2 - 3xz^2 - 3zy^2 \tag{33}$$

then solve the problem using Eqs. (6) and (7). This set up can, actually, check the accuracy of the FMM, only. The simplified mathematical model has been rigorously validated in [5]. The relative error is evaluated over all the boundary nodes using a 'global' L_2 norm error defined as

$$e = \frac{1}{|q|_{\max}} \sqrt{\frac{1}{N} \sum_{i=1}^{N} (q_i^{(e)} - q_i^{(n)})^2} \tag{34}$$

where $|q|_{\max}$ is the maximum nodal value of normal flux, the superscripts (e) and (n) refer to the exact and numerical solutions, respectively.

The relative errors as a function of the number of nodes used are presented in Fig.3. With increasing number of nodes, higher accuracy is achieved. Results also indicate that the proposed method can perform large scale computations. Therefore, it can be employed for advanced analysis of the CNT-based composites.

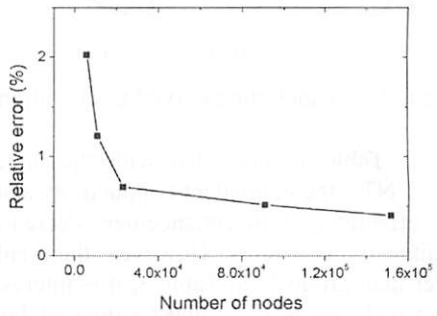

Figure 3: Relative error for normal flux.

4.2 CNT alignments in an RVE

In References [3, 4], we have performed some preliminary computations using an RVE containing one or a few short CNT(s). In this section, we carry out more advanced simulations using the proposed approach, where an RVE contains more and longer CNTs. Uniform temperatures of 300K and 200K (see Fig. 1) are imposed at the two end faces of the RVE, respectively, and heat flux free at other four side faces. This boundary condition set allows us to estimate equivalent heat conductivity of the composite in the axial direction. Using Fourier's law, the formula for equivalent heat conductivity can be written as

$$\kappa = -\frac{qL}{\Delta\phi} \tag{35}$$

where κ represents the heat conductivity; q is the heat flux density, L the length of the RVE in the axial direction and $\Delta\phi$ the temperature difference between the two end faces.

Fifteen RVEs containing different numbers of CNTs with different shapes, alignments, have been considered. These RVEs are sorted into three groups according to their shape and alignment, and presented in Figures 4-6. The first group consists of RVEs including straight CNTs in parallel alignment. In the RVEs of the second group, two more vertically aligned CNTs are added. The third group includes RVEs with curved CNTs embedded. Results of our experiments are summarized in Tables 1-3. In each table, the first row indicates the alignment of CNTs. The second, third and fourth rows list the volume fraction of CNT, equivalent heat conductivity and increase of conductivity over the matrix, respectively. To assess the enhancement effectiveness, we use as the criterion the ratio of the equivalent heat conductivity to the volume percentage, which is presented in the fifth row of each table.

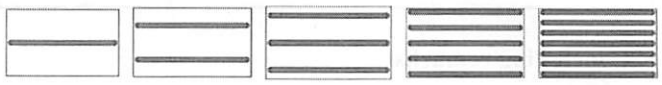

(a) (b) (c) (d) (e)

Figure 4: RVEs including straight CNTs, alignment 1.

(f) (g) (h) (i) (j)

Figure 5: RVEs including straight CNTs, alignment 2.

(k) (l) (m) (n) (o)

Figure 6: RVEs including curved CNTs, alignment 3.

Results in Table 1 show that with the increase in the number of CNTs, the equivalent conductivity also increases, while the effectiveness of enhancement decreases. Table 2 shows quite similar results. However, their enhancements are smaller than group 1. In Table 3, it is interesting to note that the case (k) gives the highest values of both the ratio and the equivalent heat conductivity, which is much higher than that obtained for models with straight CNTs. The equivalent heat conductivity is 21 times that of the polymer.

Table 1: Equivalent heat conductivities for RVEs in group 1.

RVE	(a)	(b)	(c)	(d)	(e)
Volume percentage of CNT, v	3.136%	6.272%	9.408%	15.68%	21.95%
Equivalent conductivity, κ (W/m·K)	1.646	2.890	3.780	5.079	6.114
Increase of conductivity (times)	3.5	6.8	9.2	12.7	15.5
Effectiveness of enhancement κ/v	52.49	46.08	40.18	32.39	27.85

Table 2: Equivalent heat conductivities for RVEs in group 2.

RVE	(f)	(g)	(h)	(i)	(j)
Volume percentage of CNT, r	6.381%	9.108%	11.84%	17.29%	22.74%
Equivalent conductivity, κ (W/m·K)	1.334	1.770	2.294	2.868	3.138
Increase of conductivity (times)	2.6	3.8	5.2	6.6	7.5
Effectiveness of enhancement κ/v	20.91	19.43	19.37	16.59	13.80

Table 3: Equivalent heat conductivities for RVEs in group 3.

RVE	(k)	(l)	(m)	(n)	(o)
Volume percentage of CNT, r	6.198%	8.796%	8.796%	3.553%	9.010%
Equivalent conductivity, κ (W/m·K)	7.680	7.155	7.179	1.244	1.941
Increase of conductivity (times)	20	18	18	2.4	4.2
Effectiveness of enhancement κ/v	123.9	81.34	81.62	35.02	21.54

5. Concluding remarks

In this paper, formulations of a simplified mathematical model for simulation of thermal behavior of CNT-based composites are presented. The model provides remarkable improvement in computational efficiency. The FMM is employed to further reduce the computational costs.

The proposed approach has been validated concerning a numerical example and applied to study CNT distribution in the polymer. It is concluded that dispersion of CNTs has a strong influence on the thermal properties of the composite. Some specific alignments were found that they significantly increase the equivalent heat conductivity of the composite. From the computations, one can expect that, with longer and properly aligned CNTs, it is possible to make a CNT-based composite with the heat conductivity close to that of metals.

Acknowledgements

This work was supported by the CLUSTER of Ministry of Education, Culture, Sports, Science and Technology (Japan).

References

1. Endo M., Kim Y.A., Hayashi T., Nishimura K., Matushita T., Miyashita K., Dresselhaus M.S., Vapor-grown carbon fibers: Basic properties and their battery applications, *Carbon*, **39** (2001), pp. 1287-1297.
2. Zhang J.M., Tanaka Masa., Matsumoto T., Meshless analysis of potential problems in three dimensions with the hybrid boundary node method, Int. J. Numer. Meth. Engng., **59** (2004), pp. 1147-1160.
3. Zhang J.M., Tanaka Masa., Matsumoto T., Guzik A., Heat conduction analysis in bodies containing thin-walled structures by means of Hybrid BNM with an application to CNT-based composites, JSME International Journal Series A: Solid Mechanics and Material Engineering, **47** (2004), pp. 181-188.
4. Tanaka Masa., Zhang J.M., Matsumoto T., Multi-domain Hybrid BNM for prediction of thermal properties of CNT composites, In: Honma T. and Tanaka Masa. (eds.), Proceedings of the First Asia-Pacific International Conference on Computational Methods in Engineering (ICOME 2003, Sapporo, Japan), 2003, pp. 3-12.
5. Zhang J.M., Tanaka Masa., Matsumoto T., A simplified approach for heat conduction analysis of CNT-based nano-composites, Comput. Methods Appl. Mech. Engrg., (2004), in press.
6. Rokhlin V., Rapid solution of integral equations of classical potential theory, J. Comput. Phys., **60** (1985), pp. 187-207.
7. Greengard L., Rokhlin V., A fast algorithm for particles simulations, J. Comput. Phys., **73** (1987), pp. 325-348.
8. Yoshida K., Nishimura N., Kobayashi S., Application of fast multipole Galerkin boundary integral equation method to elastostatic crack problems in 3D, Int. J. Num. Meth. Eng., **50** (2001), pp. 525-547.
9. Nishimura N., Liu Y.J., Thermal analysis of carbon-nanotube composites using a rigid-line inclusion model by the boundary integral equation method, Computational Mechanics, (2004), in press.
10. Liu Y.J., Rudolphi T.J., New identities for fundamental solutions and their applications to non-singular boundary element formulations, Computational Mechanics, **24** (1999), pp. 286-292.